# 12 DECOVALEX2019 Task C: Results of Step 2 modeling (SNL)

Teklu Hadgu, Yifeng Wang and Elena Kalinina

*Sandia National Laboratories, MS 0747, P.O. Box 5800, Albuquerque, NM 87185, (thadgu@sandia.gov, ywang@sandia.gov, eakalin@sandia.gov)*

The work for Step 1 performed at Sandia National Laboratories and reported in Section 7 has been updated to incorporate new data and to conduct new simulations using a new larger base case domain. The new simulations also include statistical analysis for different fracture realizations. A sensitivity analysis was also conducted to the study of the effect of domain size. A much larger mesh was selected to minimize boundary effects. The DFN model was upscaled to the new base case domain and the much larger domain to generate relevant permeability and porosity fields for each case. The calculations updated for Step 2 are described in Section 12.1. New calculations have also been conducted to model the flooding of the CTD and the resulting pressure recovery. The modeling includes matching of pressure and chloride experimental data at the six observation locations in Well 12MI33. The modeling was done for the 10 fracture realizations. The Step 2 recovery simulations are described in Section 12.2. The Step 2 work is summarized in Section 12.3.

## 12.1 Update of inflow modeling

In Step 1 analyses (Section 7.2) simulations were carried out for a fracture model using a Visualization Area domain, which is a CTD-scale domain. In that set-up one side of the CTD-scale domain coincided with the inlet of the inclined drift. Subsequently the base domain was enlarged to reduce boundary effects. The new base case domain size is 200 m x 300 m x 200 m, with a constant cell size of 2 m x 2m x 2m, resulting in a mesh size of 1,500,000 grid blocks. The cell size was increased to keep the same number of grid blocks as in Section 7. In this set-up the inlet to the inclined drift is away from the domain side boundaries, and the tunnel is situated near the middle of the domain.

### 12.1.1 Statistical analysis using updated fracture model

Fracture characterization for the new domain and mesh was conducted using the method detailed in Section 7.1. Figure 12.1 represents the DFN method with the tunnel and location of fracture trace data. The figure shows the CTD-scale domain and the new enlarged domain. For this study 10 DFN realizations were generated to provide a measure of uncertainty. Figures 12.2 and 12.3 show DFN permeability and aperture for one of the realizations, respectively. The DFN permeability and porosity results for the 10 realizations were upscaled to a continuum mesh for use in flow and transport simulations. Figures 12.4 and 12.5 show the upscaled permeability and porosity fields for the same realization.

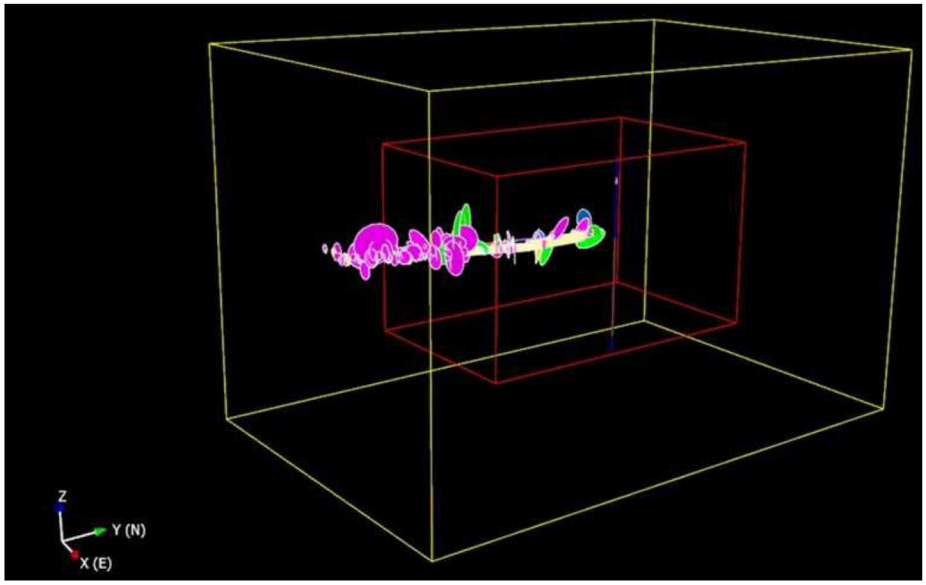


**Figure 12.1. Representation of enlarged domain with mapping of fracture traces**

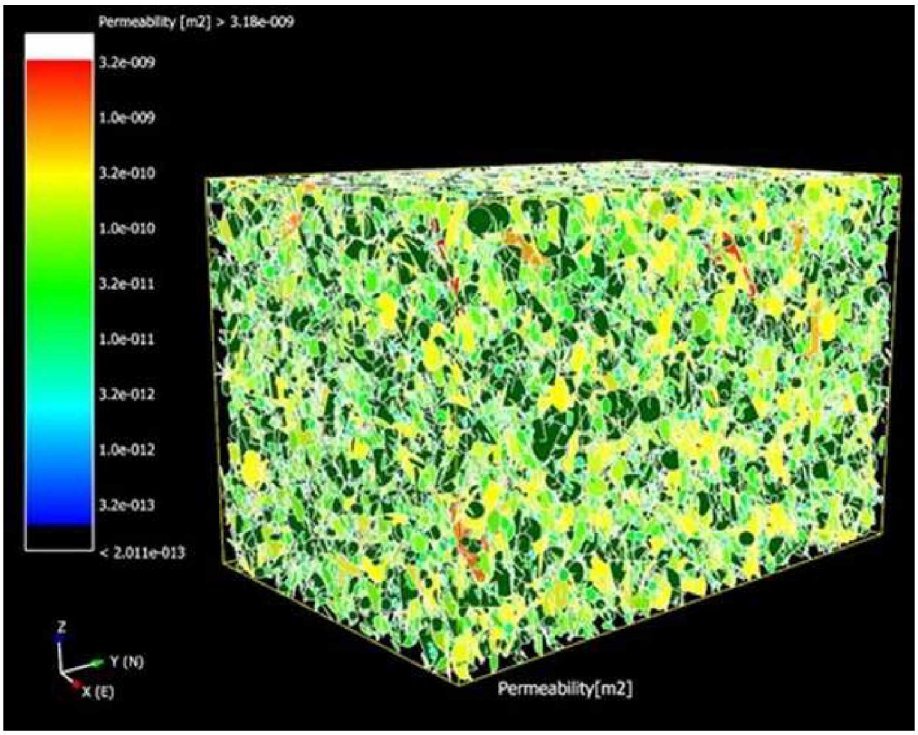


**Figure 12.2. DFN permeability field for Realization 2**

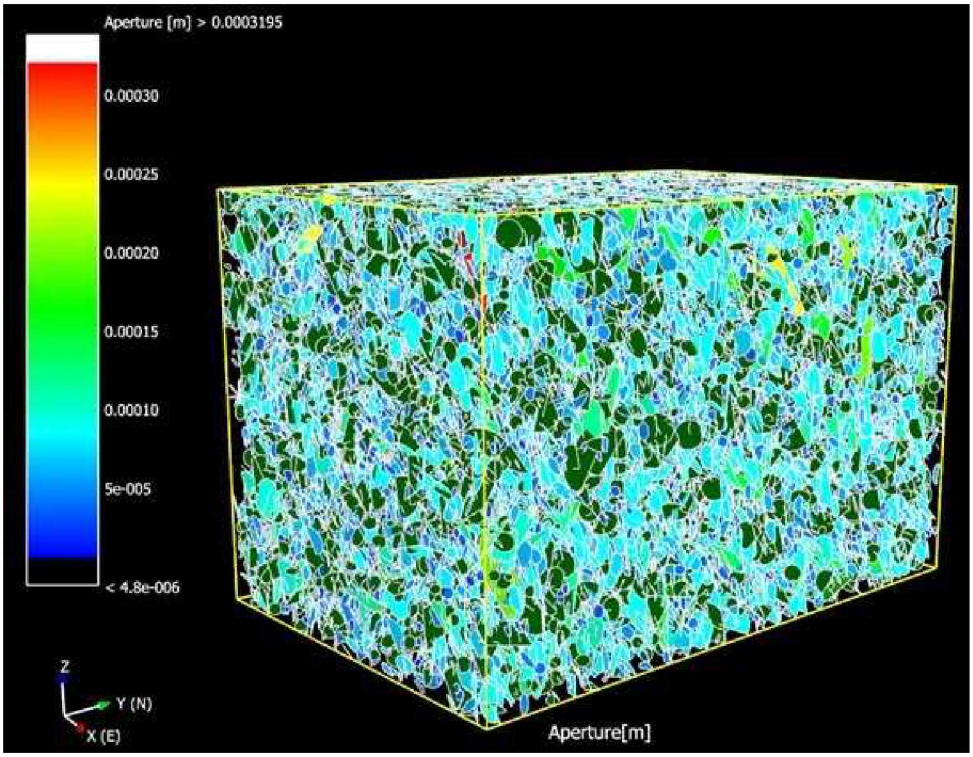


**Figure 12.3. DFN distribution of aperture for Realization 2**

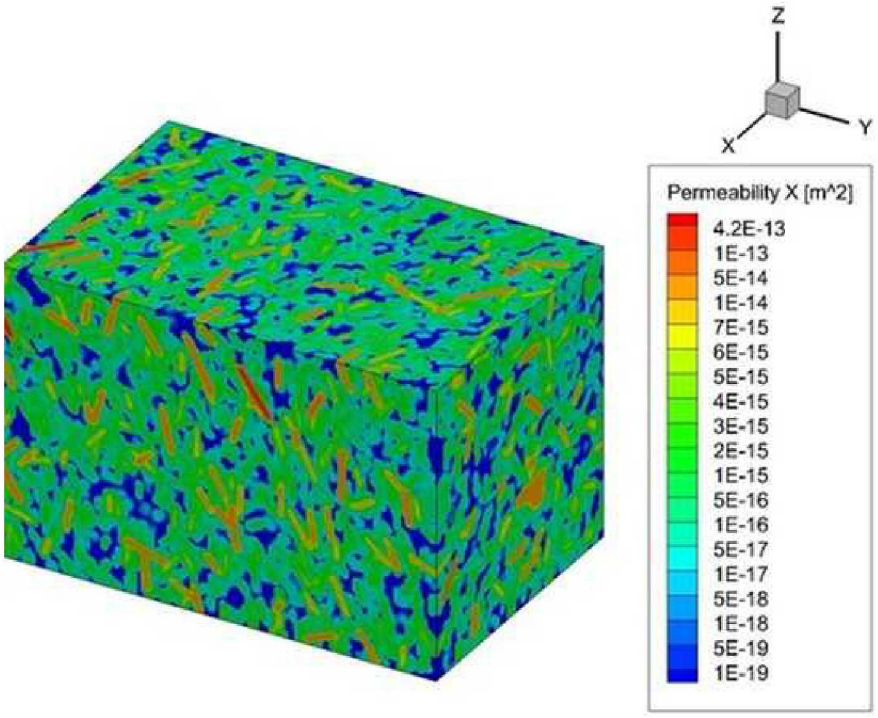


**Figure 12.4. Upscaled permeability field for Realization 2**

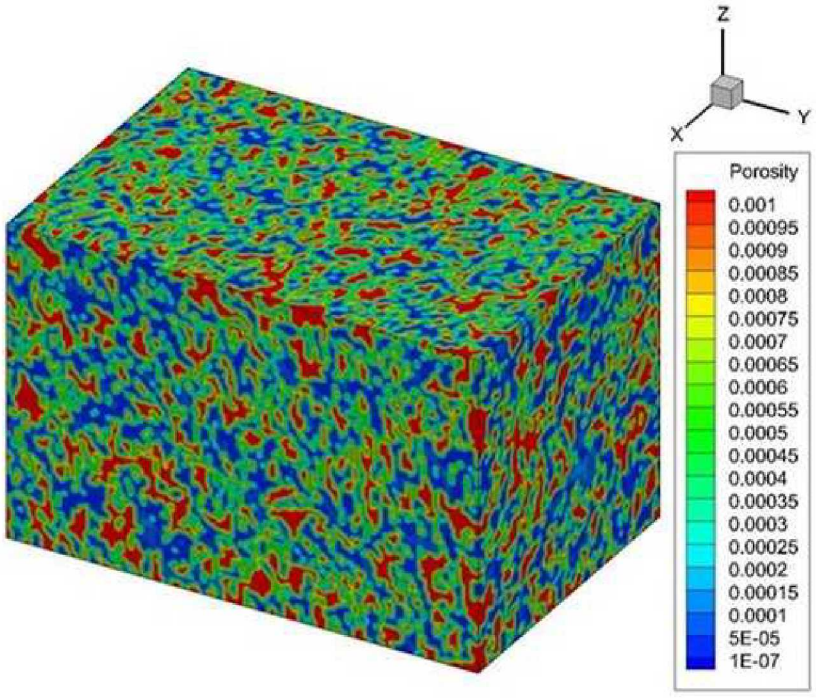


**Figure 12.5. Upscaled porosity field for Realization 2**

PFLOTRAN simulations were conducted using the method described above. An initial condition run was made with the new mesh to set hydrostatic pressure and chloride concentration gradient. As was done in Step 1 specified pressure and chloride boundary conditions were applied to the top, bottom and side domain boundaries. Figure 12.6 shows the new mesh and location of the inclined drift and CTD tunnel components. Figure 12.7 shows the steady state hydrostatic pressure used for Realization 2. Flow and transport simulations were then conducted as the excavation progressed, applying constant atmospheric pressure boundary conditions at the tunnel walls to the excavated portion of the tunnel. The simulations ran for the duration of the excavation. The output of the 10 realizations provided inflow rate and pressure predictions at observation points. Figures 12.8 to 12.11 show distribution of pressure at the end of the simulation time for Realization 2. Figure 12.8 shows a vertical slice (x-axis) at the tunnel level. Figures 12.9 and 12.10 show vertical slices (y-axis) at levels of the inclined drift and the CTD, respectively. Figure 12.11 shows a horizontal slice (z-axis) at the tunnel level. Figure 12.12 shows predictions of inflow for the 10 realizations together with experimental data points. The figure shows a better prediction of inflow for the inclined drift than the total inflow (inclined drift + CTD). Future simulations could improve the predictions when additional fracture data are incorporated in the fracture characterization method.

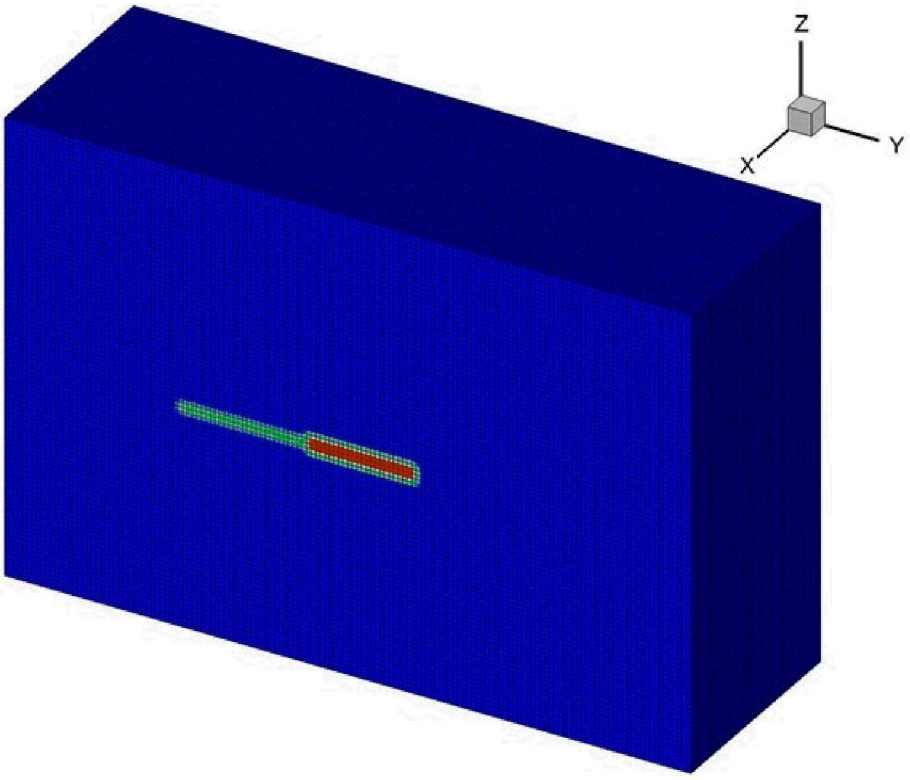


**Figure 12.6. Location of Inclined Drift and CTD**

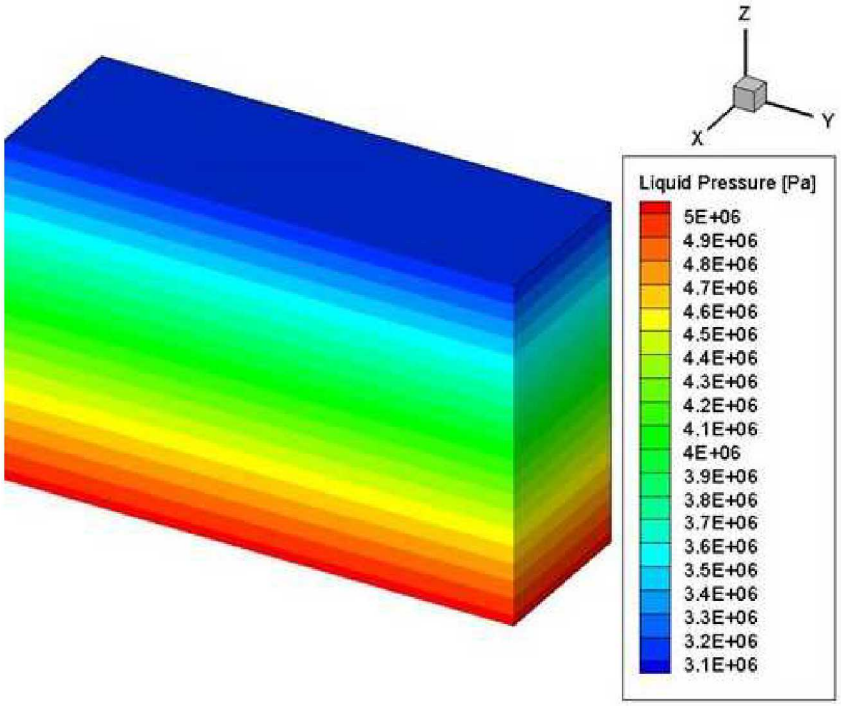


**Figure 12.7. Step2a: Steady State Pressure Distribution for Realization 2**

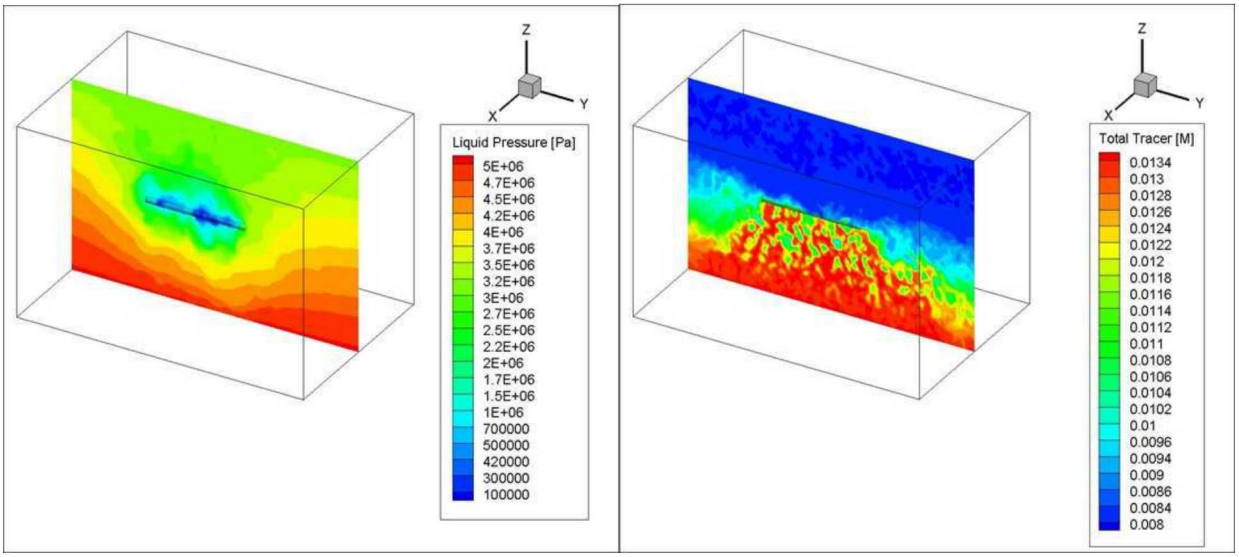


**Figure 12.8. Pressure and Chloride distribution along tunnel axis, after 173 days simulation time**

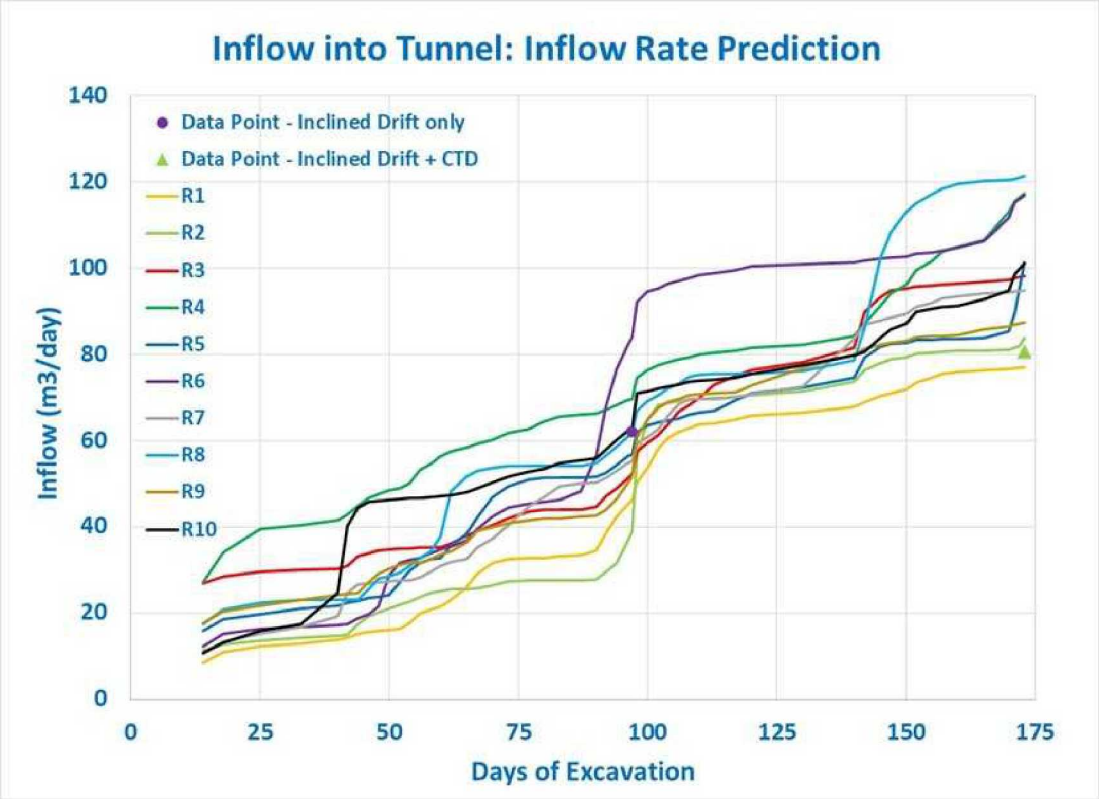


**12.9 Inflow prediction for 10 realizations using new domain**

## 12.1.2 Effect of domain size on inflow modeling

In this section the effect of the boundary conditions set for the site-scale domain is studied by changing the domain size of the base case. For this study a larger domain size was used. A 1386 m x 1486 m x 806 m (vertical) domain was selected to conduct inflow simulations. The new mesh contains 2,352,987 grid blocks. The mesh includes the original site-scale mesh together with progressively increasing grid block sizes. Discretizations of the base case mesh and the new enlarged mesh are shown in Figures 12.10 and 12.11, respectively. For the larger domain the same DFN realization as in Section 7.2 was used to produce an upscaled fracture model.

The same procedure as in Section 7.2 was followed to estimate the inflow for the larger domain. Figure 12.12 shows pressure distributions for the larger domain at the end of the simulation time (173 days). The figure shows pressure drawdown around the excavated tunnel parts due to the inflow of water as the tunnel was excavated. In this case the pressure drawdown is confined to the middle of the domain, close to the excavation, as opposed to that of the base case domain where the pressure drawdown covers a large part of the domain (Figure 12.8). Figure 12.13 shows predictions of inflow for the selected DFN realization. The plot shows predictions for the

base case domain (smaller domain) and the larger domain, together with experimental data. Much reduced inflow was predicted for the larger domain. It indicates that assigning boundary conditions not far from the tunnel influences inflow predictions. Note that for the selected realization predictions of inflow for the smaller base case domain are close to the experimental data. However, inflow predictions for several realizations using the base case domain resulted, on average, in over prediction (Figure 12.9). To get a full picture of the effect of domain size and boundary conditions there is a need to simulate inflows for all the 10 realizations using the larger domain.

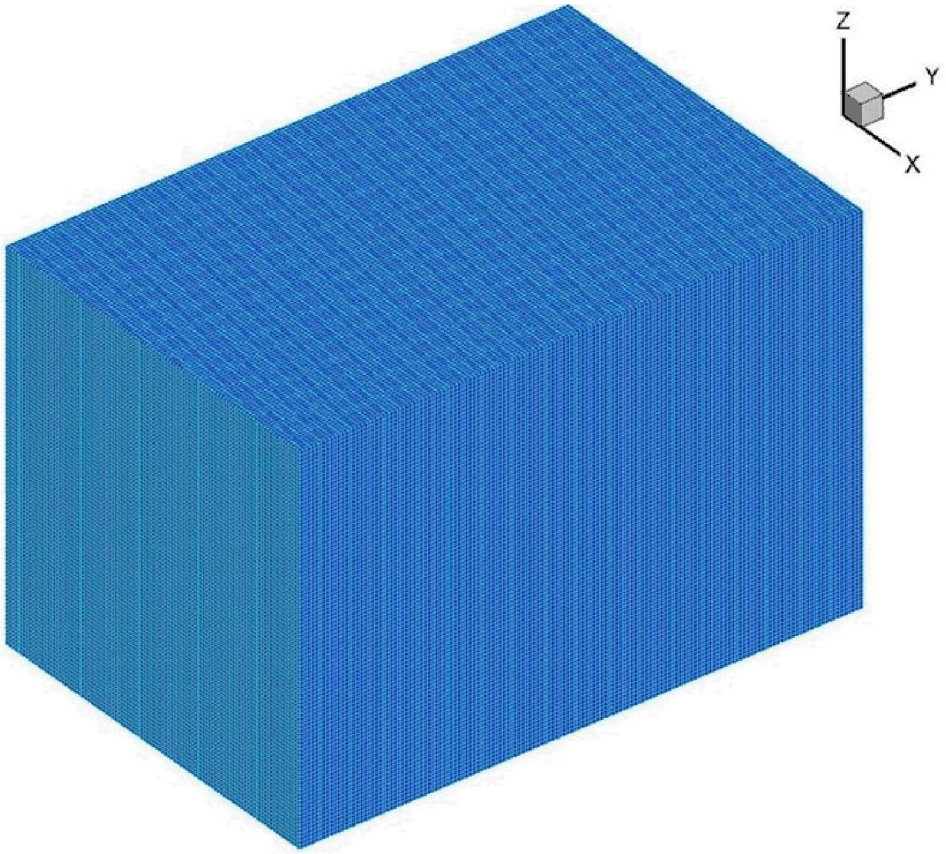


**Figure 12.10. Base case site scale domain discretization**

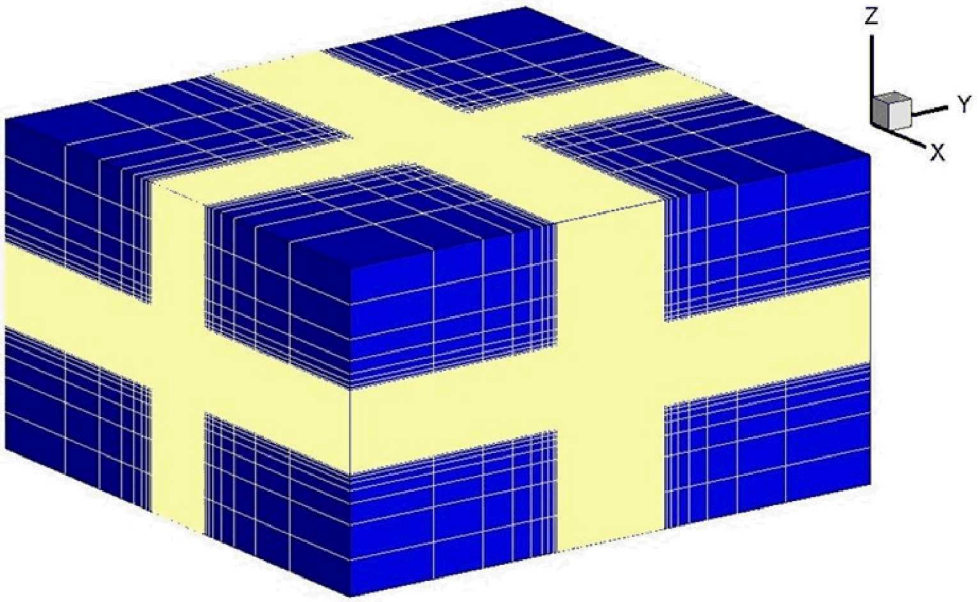


**12.11 Inflow prediction for 10 realizations using large domain**

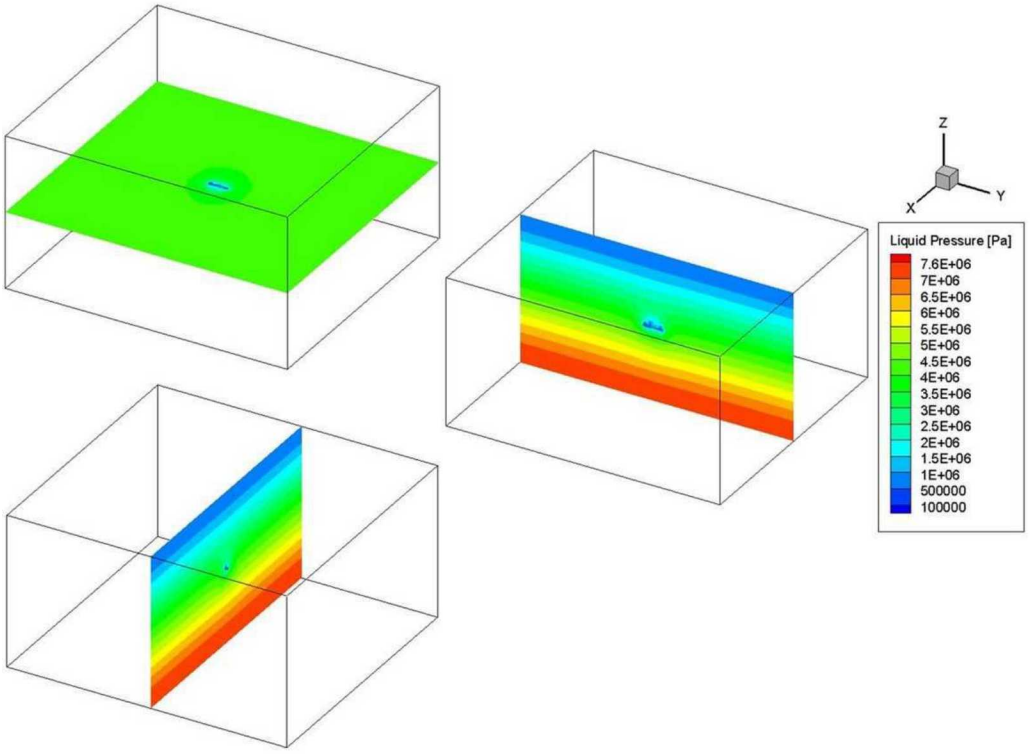


**Figure 12.12. Predicted pressure distributions for Realization 2 after 173 days simulation time for the large domain**

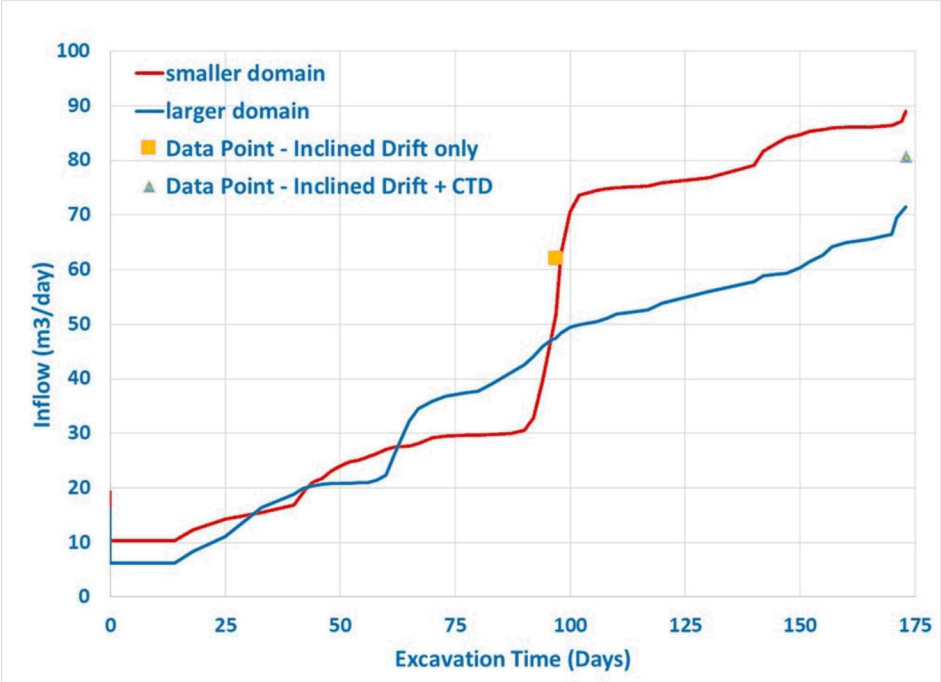


**Figure 12.13. Predicted inflow into Inclined Drift and CTD: Comparison of predictions for the base case and larger domains, together with experimental data.**

## 12.2 Modeling of recovery during water filling experiment in CTD

The GREET project conducted further flow, transport and chemical tests after the excavation of the inclined drift and the CTD. The experiments include applying of a concrete plug to isolate the CTD, filling it with water and observing hydraulic and chemical recovery following the excavation of the tunnel. The time line shown below indicates durations of major tests starting from the excavation of the tunnel.

- Incline drift and CTD excavation: 4/20/2013 to 10/14/2013
- Construction of impervious plug: 11/3/2014 to 6/2/2015
- First water-filling test (plug performance test): 8/24/2015 to 10/5/2015
- Injection of water to CTD at 500 m: 1/8/2016 to 1/25/2016
- CTD full of water: 1/25/2016 to 9/5/2017

In this section filling of the CTD with water and associated hydraulic and chemical recovery are modeled. Results of flow and non-reactive transport simulations are presented.

### 12.2.1 Modeling of flow during the recovery experiment

For the flow simulations the base case domain and mesh described in Section 12.1 were used. Because the recovery experiments were conducted in the CTD, the inclined drift was not included in the modeling. Permeability and porosity fields of Realization 2 were applied and the PFLOTRAN numerical code was used. Initial conditions were obtained by running the model using experimental initial condition data described below.

- Initial pressure at CTD: 1 atm.
- Initial pressure data at observation points in Borehole 12MI33:
    - P1 = 3.822 MPa
    - P2 = 1.286 MPa
    - P3 = 1.76 MPa
    - P4 = 3.48 MPa
    - P5 = 3.79 MPa
    - P6 = 3.357 MPa

Note that the experimental data also include data from Borehole 13MI38. These data were not used in this study because the borehole has not been included in the fracture, flow and non-reactive transport models.

Figure 12.16 shows experimental pressure recovery data provided by the GREET project. The data includes pressure history at the CTD and the observation points in the monitoring Well 12MI33. As would be expected the data show more visible pressure changes for observation points close to the CTD. JAEA project data shows that the concrete plug isolating the CTD did not function properly and that there was some leakage. The experimental leakage data are shown on the right side in Figure 12.7.

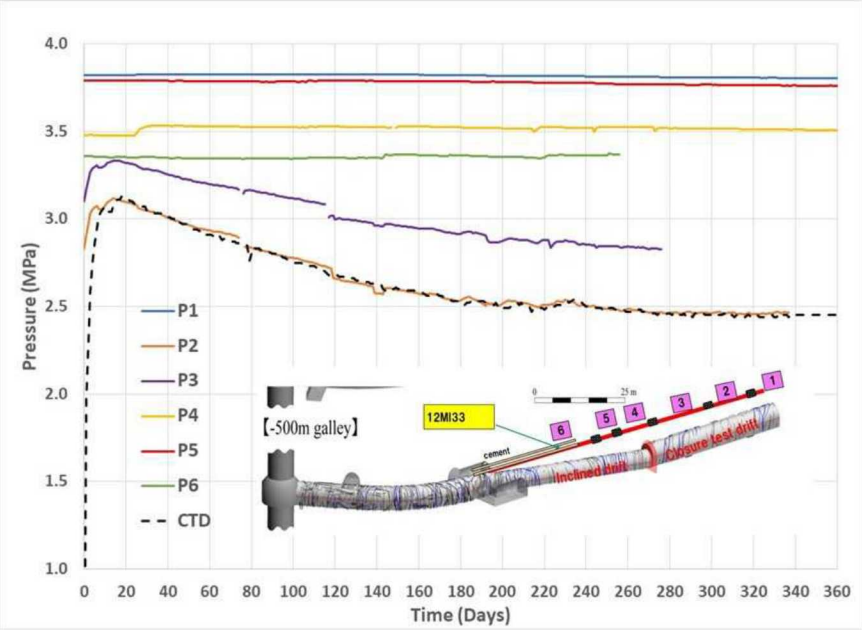


**Figure 12.14. Experimental pressure recovery data in the CTD and at observation points in Well 12MI33**

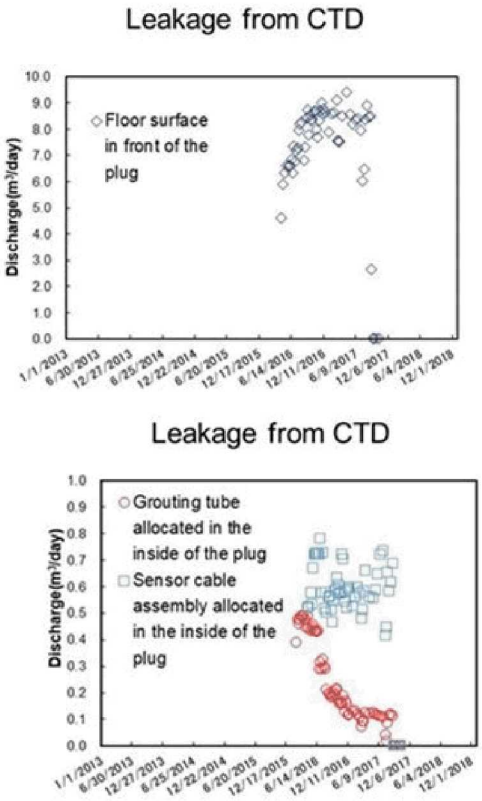


**Figure 12.15. Experimental data of leakage from CTD during recovery experiment.**

The initial condition was obtained by setting the experimental pressure values for the observation points. The flow model was then run to one year (starting Jan. 7/2016) using a steady state as initial condition. Various approaches were utilized to match the measured data. Better results were obtained by applying the experimental CTD pressure history as boundary condition at all CTD walls. The results of the simulation are shown in Figures 12.16 to 12.27. Figure 12.16 and 12.17 show pressure distributions at the beginning and end of the simulation time (360 days) for fracture Realization 2. Comparing the two figures it is evident that pressures in the CTD and the rock have somehow recovered due to the filling if the CTD.

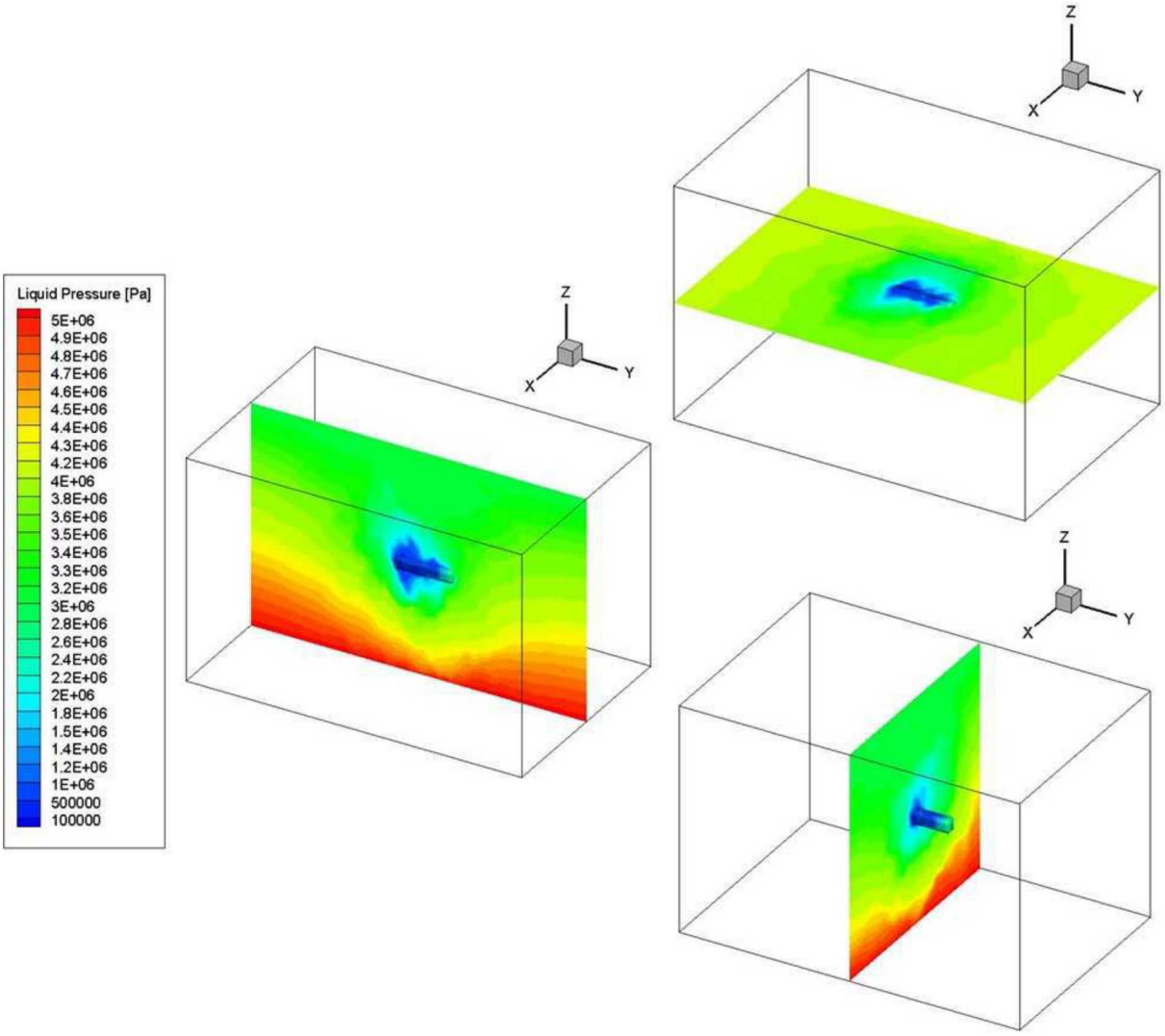


**Figure 12.16. Predicted pressure distribution along tunnel axis at the beginning of simulation for the site-scale domain. Results are for Realization 2.**

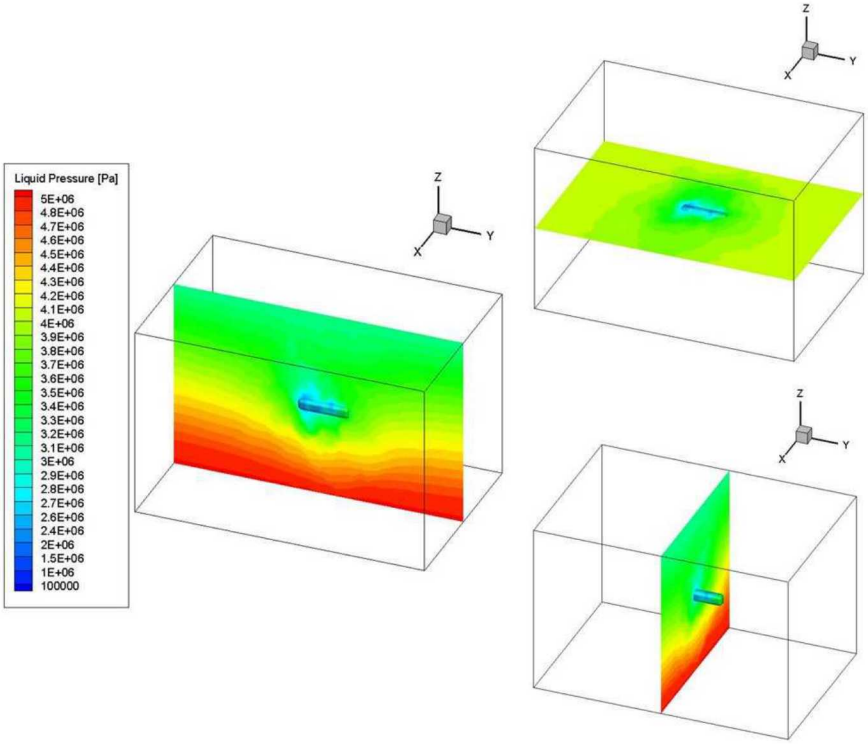


**Figure 12.17. Predicted pressure distribution along tunnel axis after 360 days simulation time for the site-scale domain. Results are for Realization 2.**

Figure 12.18 shows the predicted and experimental pressure history at the CTD during the recovery period. The simulation results are for Realization 1 and show that the imposed boundary condition at the CTD is about the same as the experimental data. Figure 12.19 shows predictions of flow at the CTD due to the imposed time varying pressure boundary condition at CTD walls for the 10 fracture Realizations. The predicted rate of flows are all negative, indicating an outflow from the CTD during the entire simulation period. The predicted negative flowrates would indicate any leakage through the concrete plug as well as outflow into the fractured rock. The magnitudes of the flowrates are larger than the measured leakage rate (Figure 12.15) which would indicate additional flow into the rock.

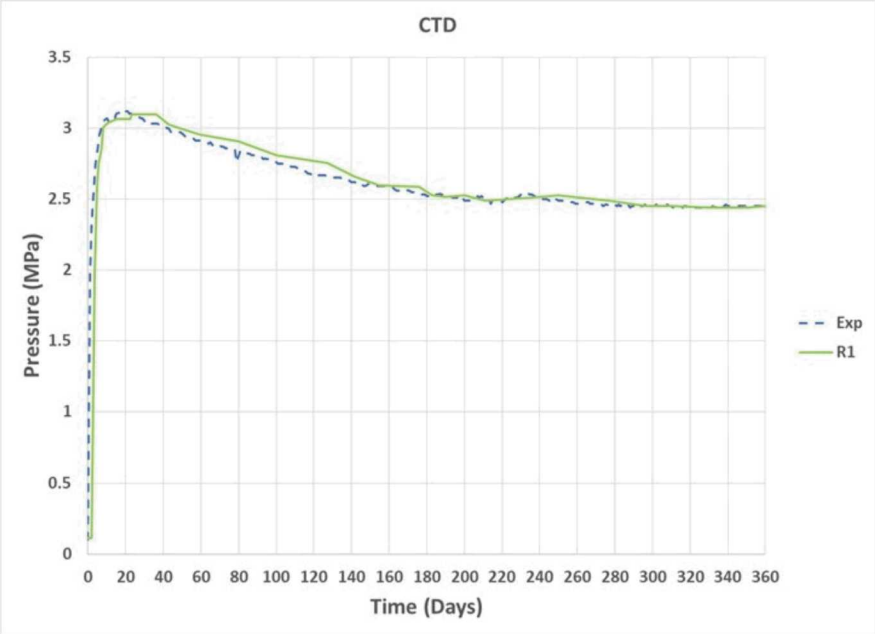


**Figure 12.18. Predicted and experimental pressure recovery at CTD**

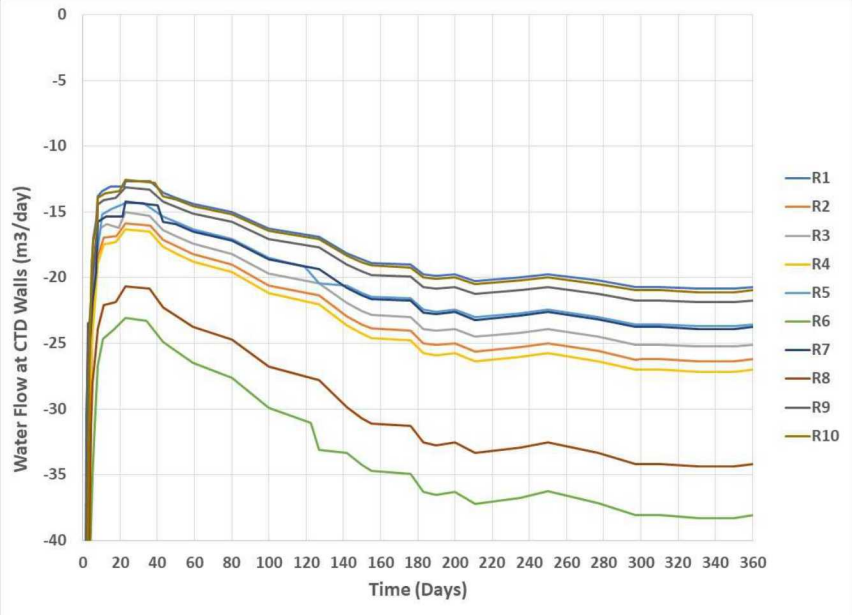


**Figure 12.19. Predicted water flow rate at CTD during recovery for Realization 2. Positive water flow rate indicates inflow into CTD and negative flow rate shows outflow (or leakage).**

Figures 12.20 to 12.25 show predictions of pressure history at the specified observation points in Well 12PI33 due to CTD water filling and post-filling pressure recovery. The figures show results for 10 fracture realizations together with the corresponding experimental data (dotted line).

Figure 12.20 shows predictions for observation point P1. The experimental pressure data for P1 shows a constant pressure throughout the recovery period. As P1 is to the right of the CTD it may not have been affected by the recovery experiment. The predicted pressure in P1 spans a range, with some of the realizations approaching the experimental data. A few of the realizations seem to have permeable connections to the CTD, resulting in lower pressures.

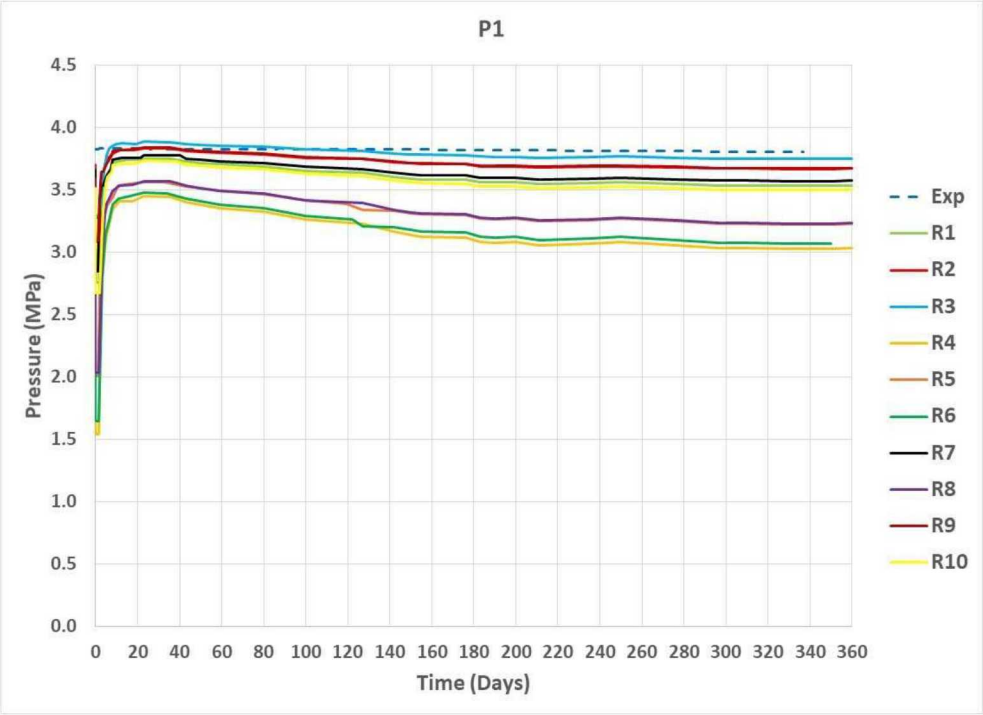


**Figure 12.20. Predicted pressure recovery at Observation Point 1 (P1) in Well 12MI33 for 10 fracture realizations. The figure also includes experimental data for P1.**

Figure 12.21 shows results for observation point P2. As shown in the figure, P2 is close to the CTD and is thus directly affected. The experimental data shows pressure decrease over time. Some of the predicted data closely match the trend. Figure 12.22 shows results for P3. As with P2, the observation point is close to the CTD. As with P2 the experimental data show pressure decrease over time. Predicted pressure of some of the realizations match the experimental data.

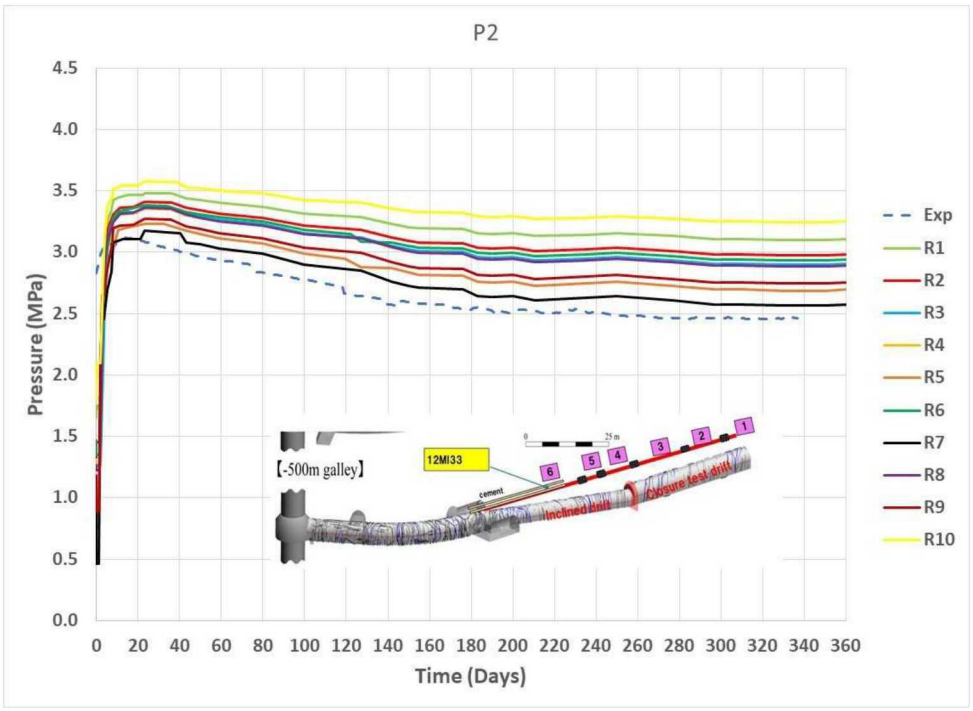


**Figure 12.21. Predicted pressure recovery at Observation Point 2 (P2) in Well 12MI33 for 10 fracture realizations. The figure also includes experimental data for P2.**

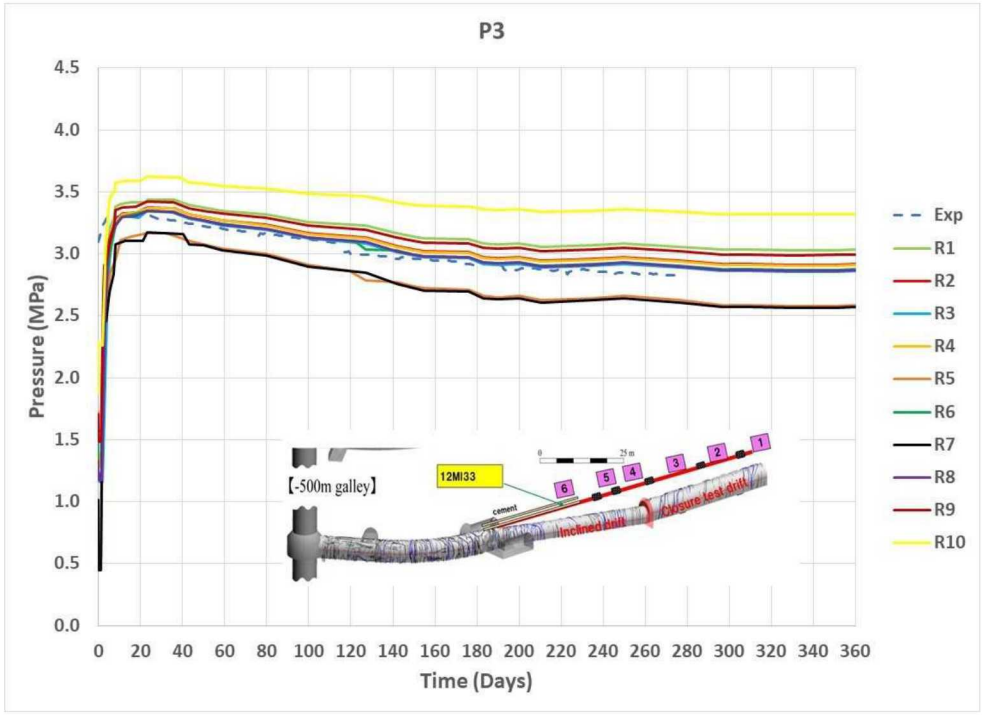


**Figure 12.22. Predicted pressure recovery at Observation Point 3 (P3) in Well 12MI33 for 10 fracture realizations. The figure also includes experimental data for P3.**

Figure 12.23 shows pressure history results for P4. The observation point is close to the left side of the CTD. The experimental data show a slight pressure decrease over time. As shown in the figure predicted pressure of some of the realizations match the experimental data. A few of the realizations may have permeable connections and thus resulted in decreased pressures. Figure 12.24 shows pressure history results for P5. The observation point is to the left of the CTD and thus may not be as influenced by the CTD filling as the points to the right of it. The experimental data shows almost constant pressure over time. Predicted pressure of almost all of the realizations match the experimental data. Figure 12.25 shows pressure history results for P6. As with P6 the observation point is further to the left of the CTD and thus may not be as influenced by the CTD filling as the points to the right of it. The experimental data show almost constant pressure over time but lower than that of P5. In this case the predicted pressure for all realizations overpredict the experimental data. Further study would be needed to understand the discrepancy.

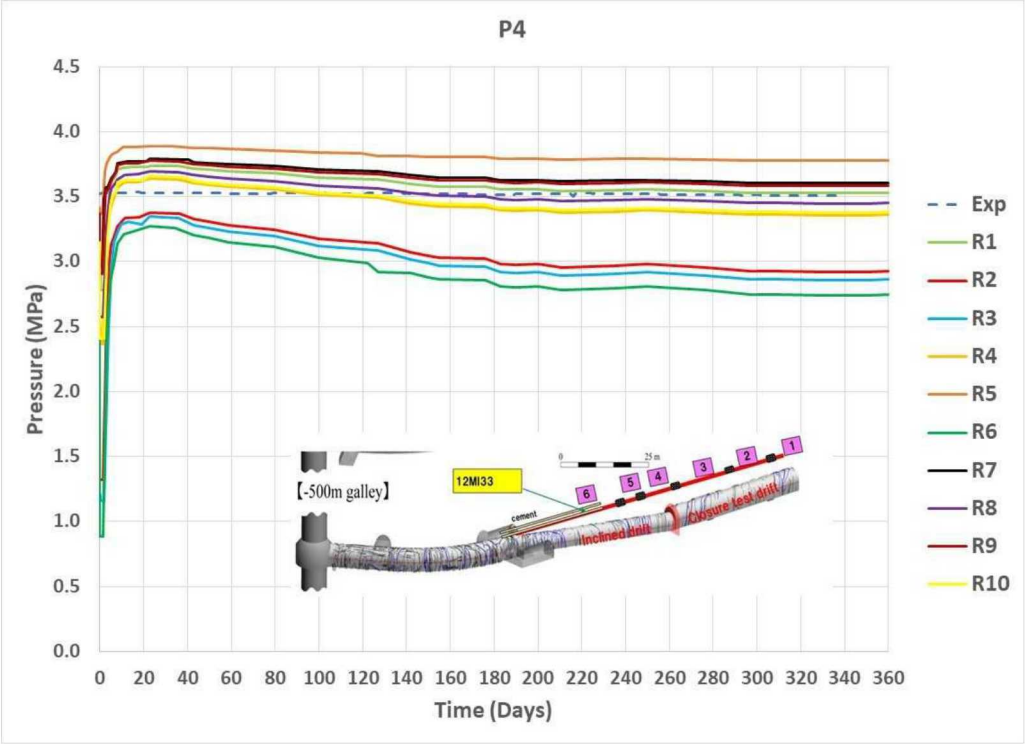


**Figure 12.23. Predicted pressure recovery at Observation Point 4 (P4) in Well 12MI33 for 10 fracture realizations. The figure also includes experimental data for P4.**

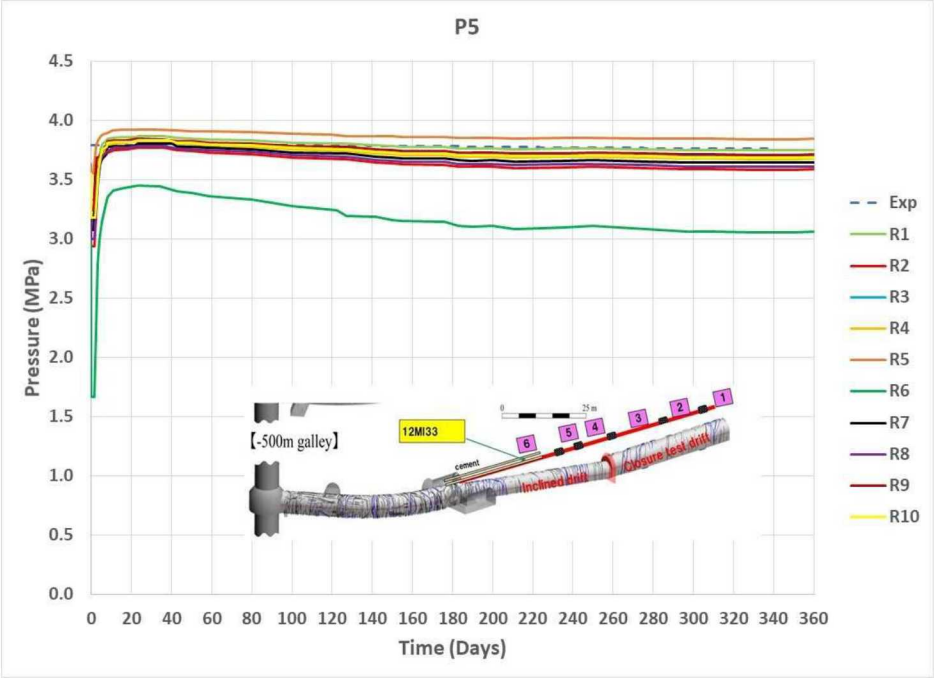


**Figure 12.24. Predicted pressure recovery at Observation Point 5 (P5) in Well 12MI33 for 10 fracture realizations. The figure also includes experimental data for P5.**

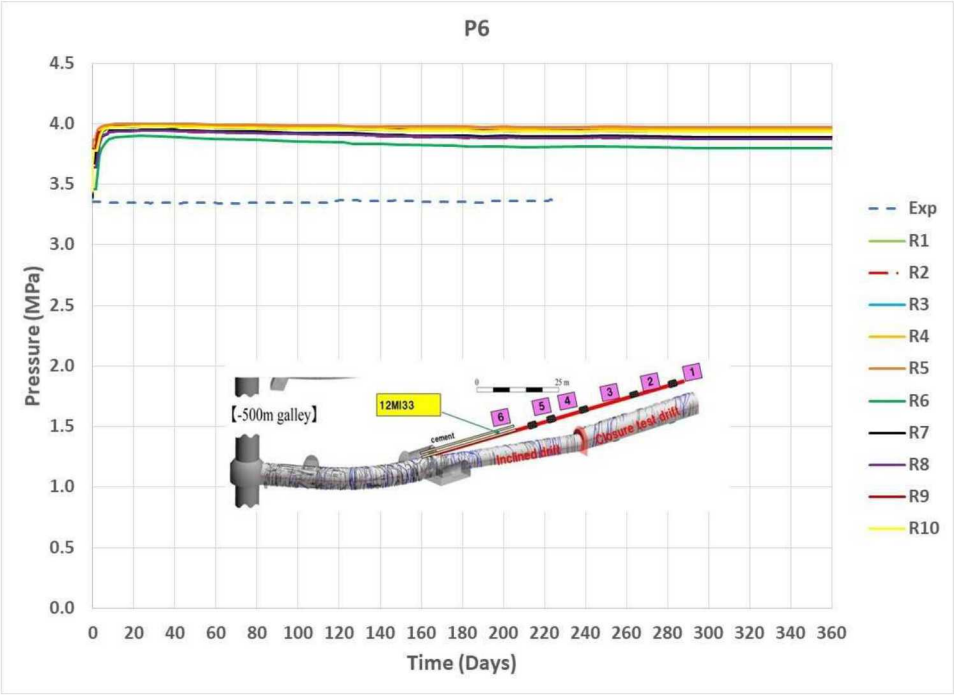


**Figure 12.25. Predicted pressure recovery at Observation Point 6 (P6) in Well 12MI33 for 10 fracture realizations. The figure also includes experimental data for P6.**

### 12.2.2 Non-reactive transport modeling during recovery experiment

For the transport simulations the same procedure as that of the flow simulations was followed. Initial conditions were obtained by running the model using experimental initial condition data described below.

- Initial chloride concentration at CTD: 475 mg/L (0.013398 M)
- Initial chloride concentration data at observation points in Borehole 12MI33:
    - P1 = 438 mg/L (0.012354 M)
    - P2 = 377 mg/L (0.010634 M)
    - P3 = 274 mg/L (0.007729 M)
    - P4 = 215 mg/L ().006064 M)
    - P5 = 594 mg/L ().016755 M)
    - P6 = 333 mg/L ().009393 M)

The above concentration data were converted to molarity for use in PFLOTRAN (given in parenthesis). The conversion equation used was:

$$Conc.\,in\,M = \frac{Conc.\,in\,mg/L}{1000\,x\,35.453}$$

with the molecular weight of chloride was 35.453 g/mol.

The initial concentrations at the CTD and the observation points in Well 12MI33 were used to generate the steady state conditions for the 10 fracture realizations. The non-reactive transport simulations then used the steady state conditions to model the recovery process. As with the flow simulations, the transport simulations used the experimental CTD chloride concentration history as boundary conditions on all the walls of the CTD. For all the transport simulations longitudinal dispersivity of 20.0 m and diffusion coefficient of $10^{-12}$ $m^2/s$ were applied. The results were sensitive to longitudinal dispersivity but a selected value was not universally applicable to model concentrations at every observation point. Thus, a value of 20.0 m was selected for this study.

Simulation results are shown in Figures 12.26 to 12.33. Figures 12.26 and 12.27 show chloride concentration distributions at the beginning and end of the simulation for Realization 2.

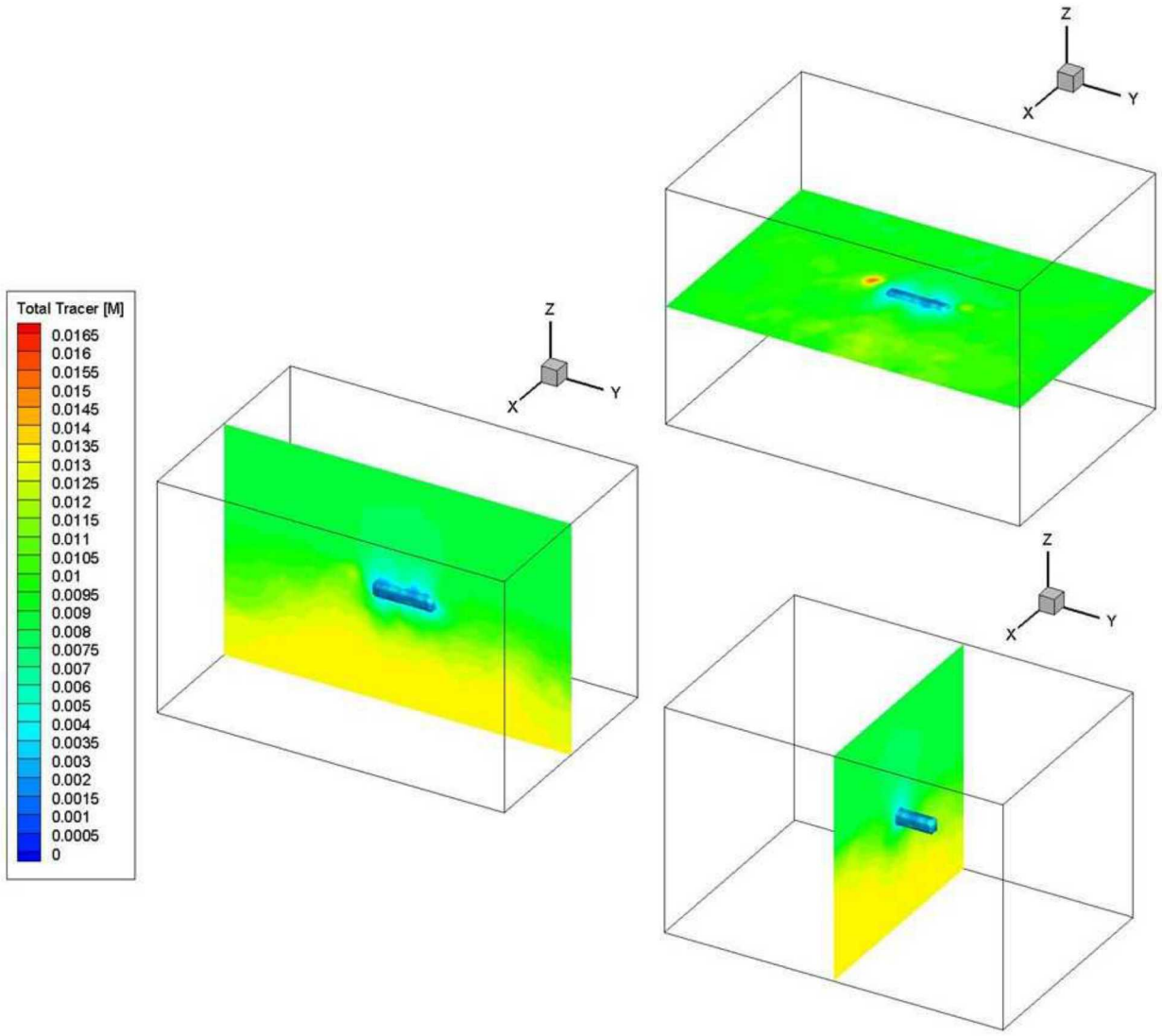


**Figure 12.26. Predicted chloride distribution along tunnel axis at the beginning of the simulation for the site-scale domain. Results are for Realization 2.**

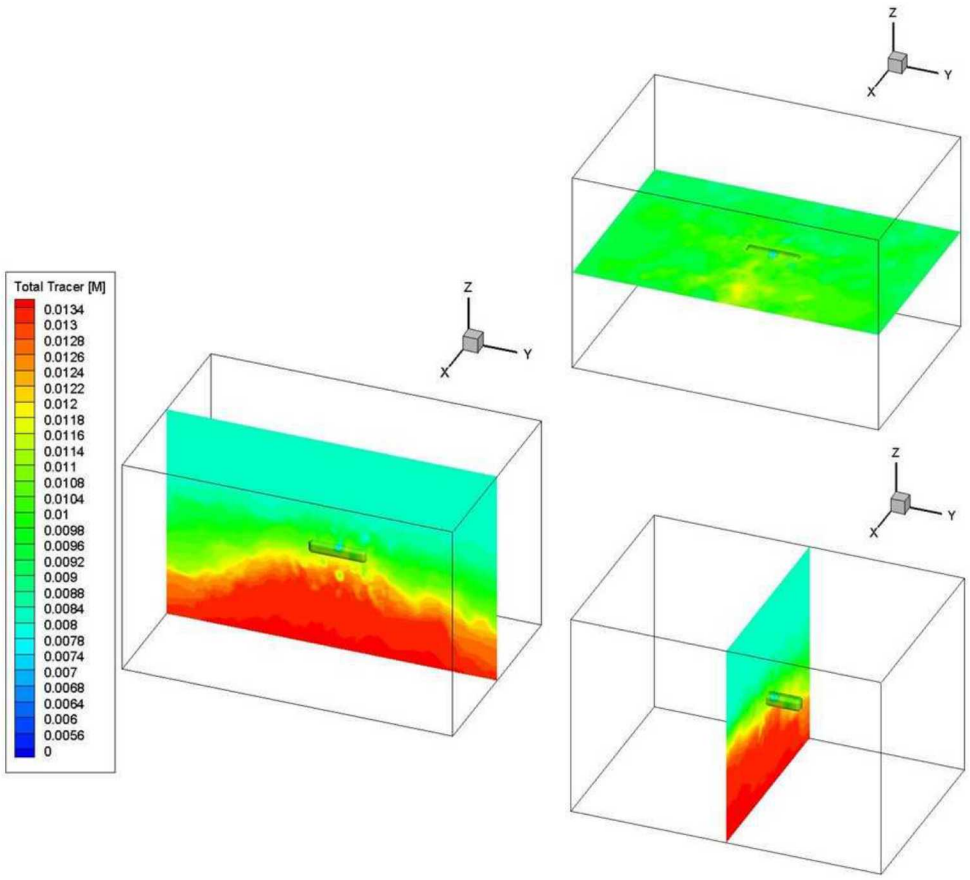


**Figure 12.27. Predicted chloride distribution along tunnel axis after 360 days simulation time for the site-scale domain. Results are for Realization 2.**

Figures 12.28 to 12.33 show predictions of chloride concentration history at the specified observation points in Well 12PI33 due to CTD water filling and post-filling pressure recovery. The figures show results for 10 fracture realizations together with the corresponding experimental data (dotted line). In general, matching chloride concentration data was not as smooth as that of pressure matching. Chloride concentrations are highly sensitive to the hydrologic changes.

Figure 12.28 shows predictions for observation point P1. All the predicted concentration results for the 10 realizations overpredict the experimental data. Some of the realizations only slightly overpredict the measure data.

Figure 12.29 shows results for observation point P2. The predicted concentrations for the 10 realizations span a wide range. However, some of the predicted data are close to the experimental data at later times. Figure 12.30 shows results for P3. As with P2, the observation point is close to the CTD. The predictions are similar to that of P2.

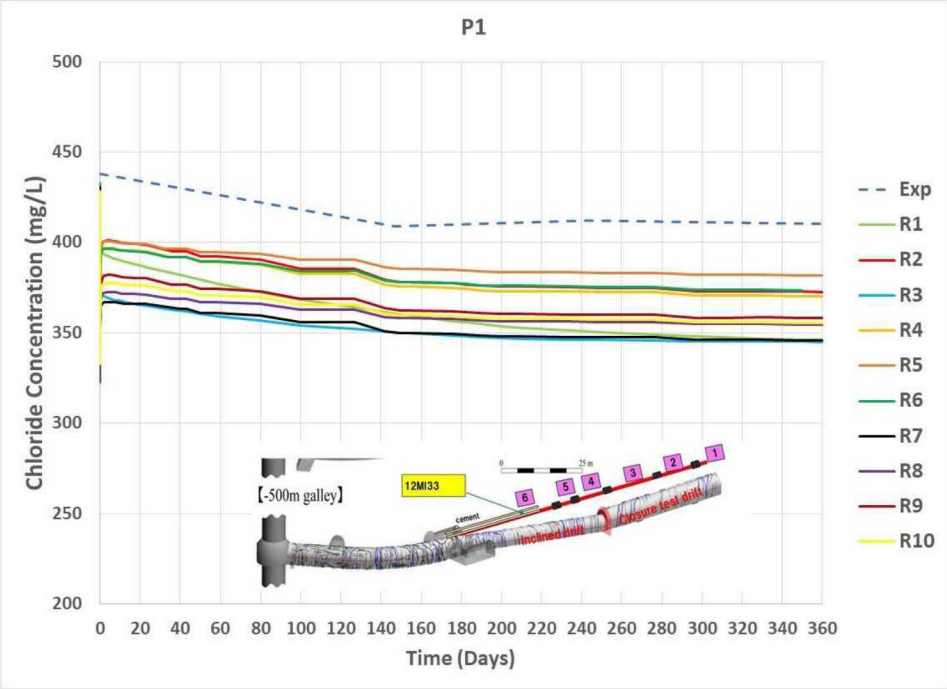


**Figure 12.28. Predicted chloride concentration during recovery at Observation Point 1 (P1) in Well 12MI33 for 10 fracture realizations. The figure also includes experimental data for P1.**

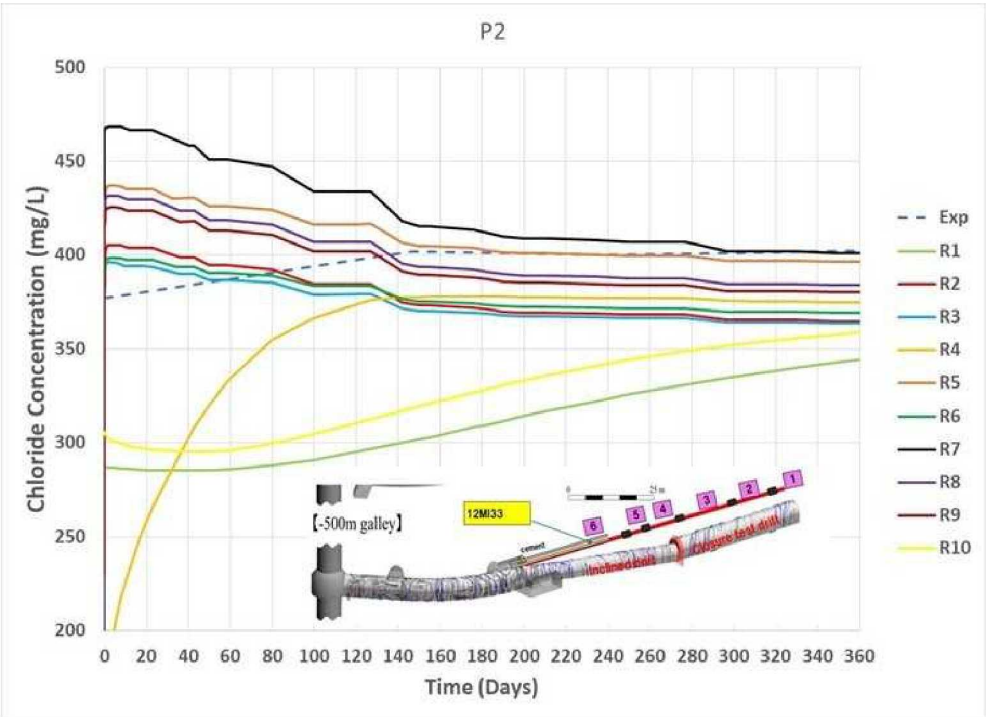


**Figure 12.29. Predicted chloride concentration during recovery at Observation Point 2 (P2) in Well 12MI33 for 10 fracture realizations. The figure also includes experimental data for P2.**

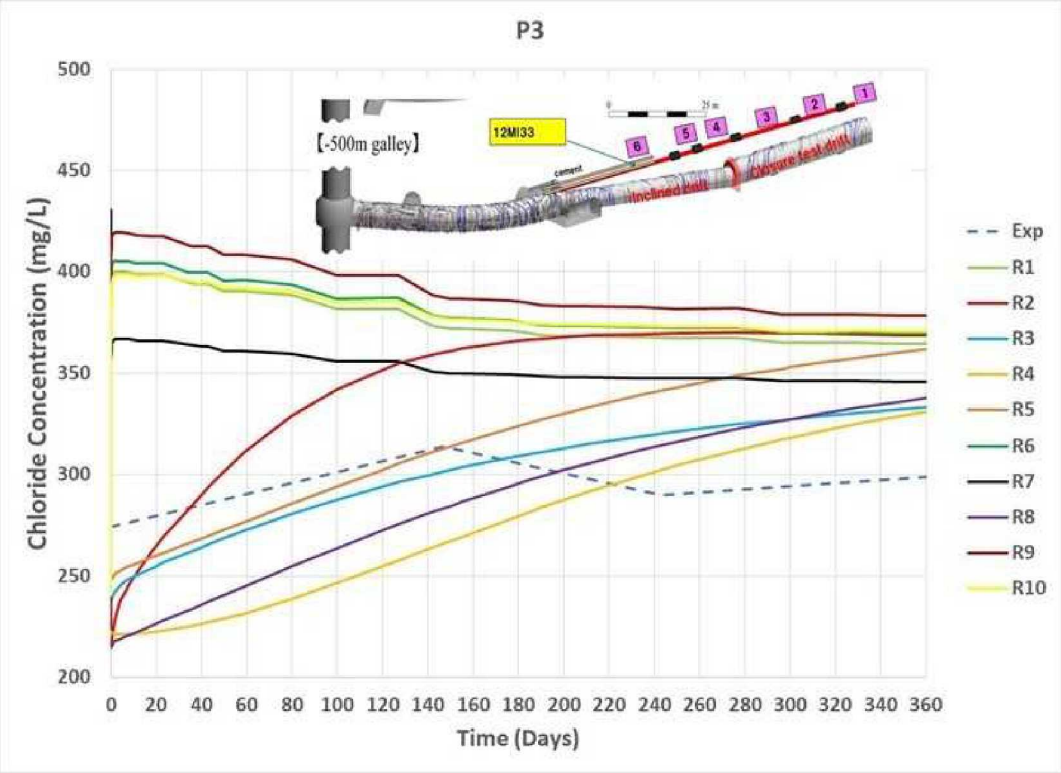


**Figure 12.30. Predicted chloride concentration during recovery at Observation Point 3 (P3) in Well 12MI33 for 10 fracture realizations. The figure also includes experimental data for P3.**

Figure 12.31 shows chloride concentration history results for P4. The observation point is close to the left side of the CTD. The results show that the predictions for all the realizations overpredict the experimental data.

Figure 12.32 shows pressure history results for P5. The observation point is to the left of the CTD. The experimental data show much higher concentrations compared to the other observation points. It is not clear why the chloride concentrations are out of step while the pressure data are consistent with the other observation points. As would be expected, the predicted concentration values consistently underpredicted the experimental data. Additional analysis of the experimental data would be needed to address such an anomaly.

Figure 12.33 shows chloride concentration history results for P6. The observation point is further to the left side of the CTD. The results show that the predictions for all the realizations slightly overpredict the experimental data. The predictions are much better than that of P5.

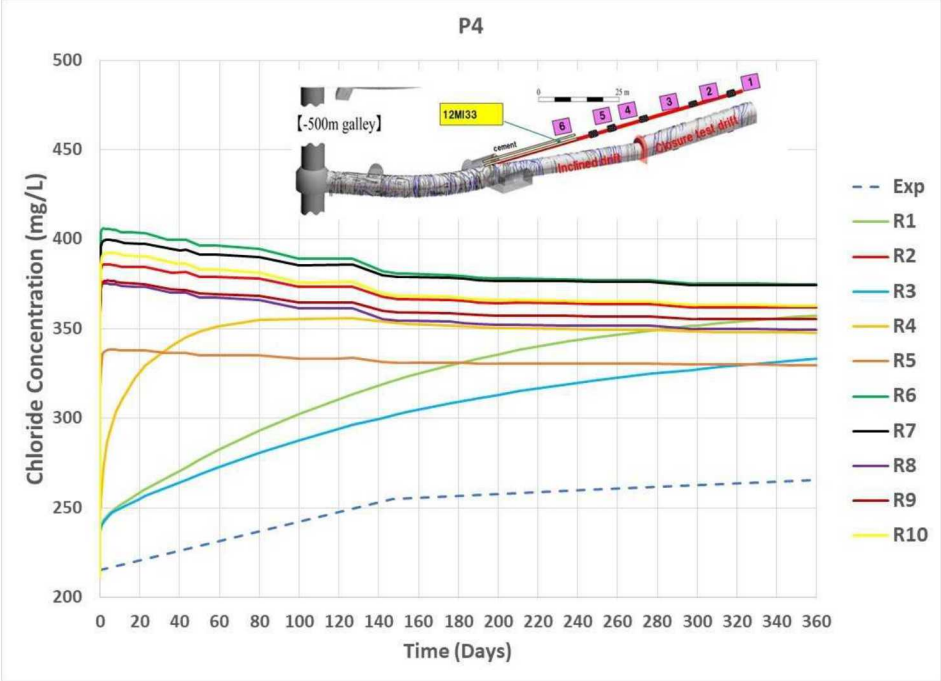


**Figure 12.31. Predicted chloride concentration during recovery at Observation Point 4 (P4) in Well 12MI33 for 10 fracture realizations. The figure also includes experimental data for P4.**

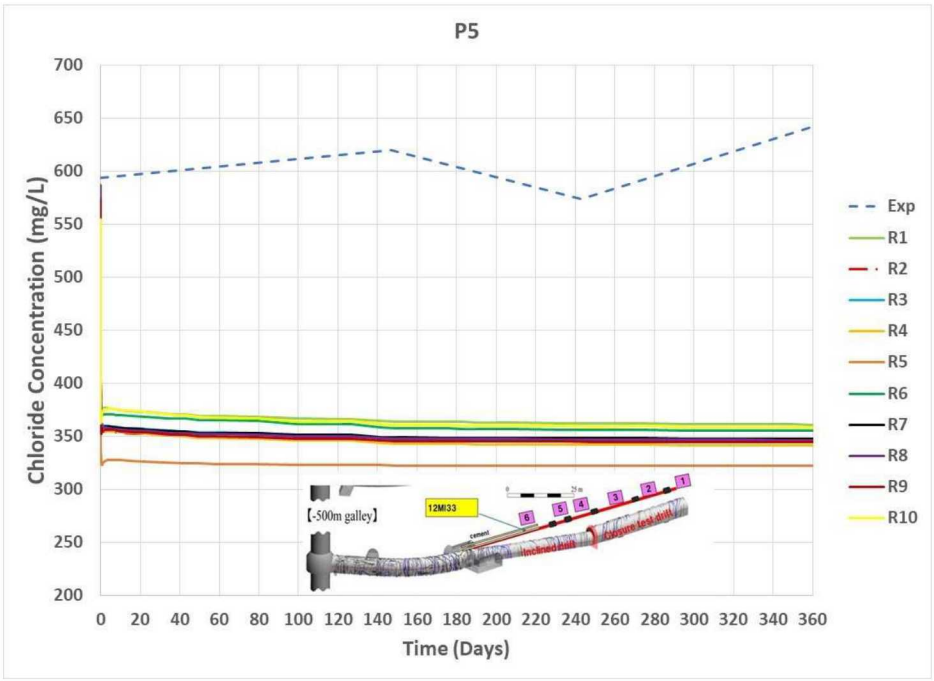


**Figure 12.32. Predicted chloride concentration during recovery at Observation Point 5 (P5) in Well 12MI33 for 10 fracture realizations. The figure also includes experimental data for P5.**

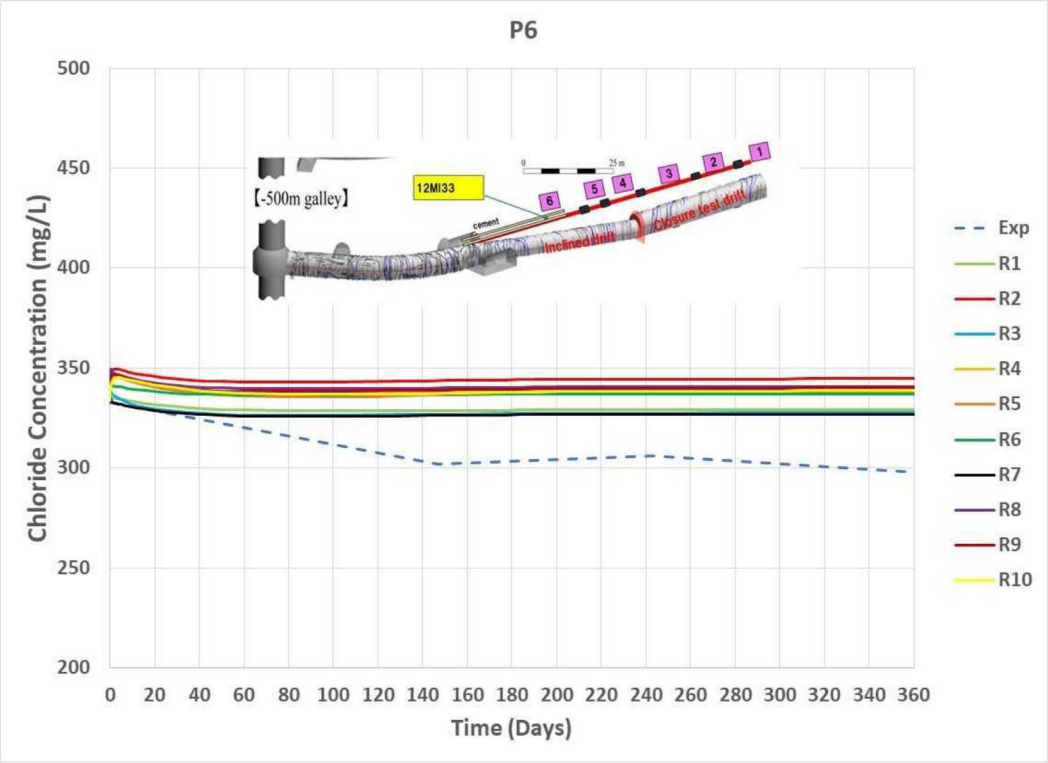


**Figure 12.33. Predicted chloride concentration during recovery at Observation Point 6 (P6) in Well 12MI33 for 10 fracture realizations. The figure also includes experimental data for P6.**

## 12.3 Summary of Step 2 flow and non-reactive transport modeling

Modeling analyses were conducted on DECOVALEX19, Task C, Step 2. For Step 2, the analysis was based on a larger domain to reduce boundary effects. The analysis also included fracture characterization using the new domain. The fracture model produced 10 DFN realizations which were upscaled to a continuum mesh for use in flow and transport. Boundary and initial conditions specified by the project were applied to flow and transport simulations. Project experimental data of excavation progress were also used. The simulation method previously developed and reported in Step 1 to simulate excavation progress by continuously removing material from the excavated area was utilized. The DAKOTA statistical analysis and optimization code and the PFLOTRAN numerical flow and transport code were used. Predictions of inflow into the inclined drift for the 10 realizations are reasonable when compared with the experimental data. Inflow of the combined inclined drift and CTD were largely overpredicted. This could be due to boundary effects as a result of the selected base case domain. The simulations provided statistical data with uncertainty range.

The analyses also included a study of domain size by comparing inflow results for the base case domain (200 m x 300 m x 200 m) with that of a much larger domain (1386 m x 1486 m x 806 m). The comparisons were done for a single fracture realization. Pressure distribution simulation results show that the site-scale domain exhibited boundary effects while the larger domain had no such effects. The inflow results for the two domains also differ. To get a more complete picture the inflow comparison would need to include all 10 fracture realizations.

Simulations were also made to model water filling of the plugged CTD and pressure recovery. For the analysis the base case domain with domain size of 200 m x 300 m x 200 m was used. The 10 upscaled fracture realizations were also used to provide permeability and porosity distributions. Boundary and initial conditions specified by the project were applied to flow and transport simulations. Simulation results were compared with project experimental data. The results show that pressure predictions of many of the 10 realizations closely match the experimental data at the observation points in Well 12MI33. The predictions of chloride concentrations were not as close as the pressure predictions. Further study would be needed to understand all the discrepancies.

Future simulations could improve the predictions when additional fracture data (Borehole 13MI38) are incorporated in the fracture characterization method. It is also important to incorporate any damage around the tunnel as such data could influence local variations in pressure and chloride concentration. The transport results were also sensitive to longitudinal dispersivity but a selected value was not universally applicable to model concentrations at every observation point. Further examination of this would help identify the local flow and transport characteristics.

# Acknowledgements

Sandia National Laboratories is a multimission laboratory managed and operated by National Technology and Engineering Solutions of Sandia LLC, a wholly owned subsidiary of Honeywell International Inc., for the U.S. Department of Energy's National Nuclear Security Administration under contract DE-NA0003525.

DECOVALEX *is an international research project comprising participants from industry, government and academia, focusing on development of understanding, models and codes in complex coupled problems in sub-surface geological and engineering applications; DECOVALEX-2019 is the current phase of the project. The authors appreciate and thank the DECOVALEX-2019 Funding Organizations ADRA, BGR/UFZ, CNSC, US DOE, ENSI, JAEA, IRSN, KAERI, NWMO, RWM, SÚRAO, SSM and Taipower for their financial and technical support of the work described in this paper. The statements made in the paper are, however, solely those of the authors and do not necessarily reflect those of the Funding Organizations*